

## Thiols in the ISM: first detection of HC(O)SH and confirmation of C<sub>2</sub>H<sub>5</sub>SH

LUCAS F. RODRÍGUEZ-ALMEIDA,<sup>1</sup> IZASKUN JIMÉNEZ-SERRA,<sup>1</sup> VÍCTOR M. RIVILLA,<sup>1,2</sup> JESÚS MARTÍN-PINTADO,<sup>1</sup>  
SHAOSHAN ZENG,<sup>3</sup> BELÉN TERCERO,<sup>4</sup> PABLO DE VICENTE,<sup>4</sup> LAURA COLZI,<sup>1,2</sup> FERNANDO RICO-VILLAS,<sup>1</sup> SERGIO MARTÍN,<sup>5,6</sup>  
AND MIGUEL A. REQUENA-TORRES<sup>7,8</sup>

<sup>1</sup>*Centro de Astrobiología (CSIC-INTA), Ctra Ajalvir km 4, 28850, Torrejón de Ardoz, Madrid, Spain*

<sup>2</sup>*INAF-Osservatorio Astrofisico di Arcetri, Largo Enrico Fermi 5, 50125, Florence, Italy*

<sup>3</sup>*Star and Planet Formation Laboratory, Cluster for Pioneering Research, RIKEN, 2-1 Hirosawa, Wako, Saitama, 351-0198, Japan*

<sup>4</sup>*Observatorio de Yebes (IGN), Cerro de la Palera s/n, 19141, Guadalajara, Spain*

<sup>5</sup>*European Southern Observatory, Alonso de Córdova 3107, Vitacura 763 0355, Santiago, Chile*

<sup>6</sup>*Joint ALMA Observatory, Alonso de Córdova 3107, Vitacura 763 0355, Santiago, Chile*

<sup>7</sup>*University of Maryland, College Park, ND 20742-2421, USA*

<sup>8</sup>*Department of Physics, Astronomy and Geosciences, Towson University, MD 21252, USA*

### ABSTRACT

The chemical compounds carrying the thiol group (-SH) have been considered essential in recent prebiotic studies regarding the polymerization of amino acids. We have searched for this kind of compounds toward the Galactic Centre quiescent cloud G+0.693-0.027. We report the first detection in the interstellar space of the trans-isomer of monothioformic acid (t-HC(O)SH) with an abundance of  $\sim 1 \times 10^{-10}$ . Additionally, we provide a solid confirmation of the gauche isomer of ethyl mercaptan (g-C<sub>2</sub>H<sub>5</sub>SH) with an abundance of  $\sim 3 \times 10^{-10}$ , and we also detect methyl mercaptan (CH<sub>3</sub>SH) with an abundance of  $\sim 5 \times 10^{-9}$ . Abundance ratios were calculated for the three SH-bearing species and their OH-analogues, revealing similar trends between alcohols and thiols with increasing complexity. Possible chemical routes for the interstellar synthesis of t-HC(O)SH, CH<sub>3</sub>SH and C<sub>2</sub>H<sub>5</sub>SH are discussed, as well as the relevance of these compounds in the synthesis of prebiotic proteins in the primitive Earth.

*Keywords:* Astrochemistry—Chemical abundance—Interstellar molecules—Galactic Centre

### 1. INTRODUCTION

Among different theories of origin of life, one recurrent conundrum is the abiotic polymerization of amino acids since it requires ribosomes, macromolecular machines containing ribonucleic acid (RNA) and proteins. How could the first proteins form if they were needed to synthesize others? Following the ideas of Foden et al. (2020), a possible solution involves a thiol-based scenario in which SH-bearing molecules, together with the family of thioacids (R-C(O)SH) and thioesters (R-S-R'), have important properties as energy carriers and catalysts (Chandru et al. 2016; Leman et al. 2017). Although these types of compounds could be created in-situ by an H<sub>2</sub>S-mediated chemistry under prebiotically plausible conditions on early Earth (Shalayel et al. 2020), they also could have been delivered exogenously. Hence, observations of thiol-based molecules in space could shed some light on the availability of such compounds on a primitive Earth, and on their role in the prebiotic synthesis of proteins.

More than 220 molecules have been detected in the interstellar medium (ISM) and circumstellar shells<sup>1</sup> to date. However, sulfur-containing species only account for 20 of them. Furthermore, while molecules detected carrying C, H or N range from 2 up to 13 atoms, the vast majority of S-bearing molecules have, at most, 4 atoms (such as H<sub>2</sub>CS; Sinclair et al. 1973). This could be due to the relatively low cosmic abundance of atomic sulfur ( $\approx 10^{-5}$  with respect to H<sub>2</sub>, that is, more than 10 times lower than C or O; Asplund et al. 2009) together with its ability to have many different oxidation states and allotropes when compared to the more abundant elements (Jiménez-Escobar et al. 2014; Shingledecker et al. 2020) and its capacity of depleting fast in dense molecular clouds (Laas et al. 2019).

Corresponding author: Lucas F. Rodríguez-Almeida  
lrodriguez@cab.inta-csic.es

<sup>1</sup> <https://cdms.astro.uni-koeln.de/classic/molecules>

As a consequence, a very few S-bearing molecules containing more than 4 atoms have firmly been detected in the ISM so far. One example is methyl mercaptan (hereafter  $\text{CH}_3\text{SH}$ ), which has been detected in several environments, such as pre-stellar cores (Gibb et al. 2000), massive star-forming regions like Sagittarius B2 (Linke et al. 1979; Müller et al. 2016), and Solar-like protostars (Majumdar et al. 2016). The other one is ethyl mercaptan (hereafter  $\text{C}_2\text{H}_5\text{SH}$ ) which was tentatively detected toward Orion KL (Kolesníková et al. 2014). Other searches for complex S-bearing molecules were unsuccessful, such as  $\text{CH}_3\text{CHS}$  (thioacetaldehyde; Margulès et al. 2020),  $\text{NH}_2\text{CHS}$  (thioformamide; Motiyenko et al. 2020) and  $\text{CH}_3\text{SC}(\text{O})\text{H}$  (S-methyl thioformate; Jabri et al. 2020).

In this Letter, we report the first detection in the ISM of the trans isomer of monothioformic acid (hereafter  $\text{HC}(\text{O})\text{SH}$ ), the simplest thiol acid. We also report a solid confirmation of the gauche isomer of  $\text{C}_2\text{H}_5\text{SH}$ , together with the detection of  $\text{CH}_3\text{SH}$ . These molecules are found toward the quiescent Giant Molecular Cloud G+0.693-0.027 located in the Galactic Center (hereafter G+0.693). This source shows a very rich chemistry with up to 40 different complex organic molecules (COMs<sup>2</sup>) detected (see, for example: Requena-Torres et al. 2008; Zeng et al. 2018; Rivilla et al. 2018, 2019, 2020; Jiménez-Serra et al. 2020). Studies suggest that this cloud could be undergoing a cloud-cloud collision (Zeng et al. 2020), which induces large-scale shocks that sputter dust grains and that enhance the gas-phase abundance of molecules by several orders of magnitude (Requena-Torres et al. 2006).

## 2. OBSERVATIONS

We have used a spectral line survey toward G+0.693 covering several windows between 32 GHz to 172 GHz with an average resolution of  $1.5 \text{ km s}^{-1}$ , although the final spectral resolution employed in the figures has been smoothed up to  $3 \text{ km s}^{-1}$ . We stress that this is for a proper line visualization and does not alter in any form the analysis done.

For the observations, we used both the IRAM 30m telescope located at Pico Veleta (Granada, Spain) and the Yebes 40m telescope<sup>3</sup> (Guadalajara, Spain). The equatorial coordinates of the molecular cloud G+0.693 are  $\alpha(\text{J2000.0}) = 17^{\text{h}}47^{\text{m}}22^{\text{s}}$ , and  $\delta(\text{J2000.0}) = -28^{\circ}21'27''$ . The position switching mode was used in all the observations with the off position located at  $(-885'', 290'')$  from the source. The line intensity of the spectra was measured in units of  $T_{\text{A}}^*$  as the molecular emission toward G+0.693 is extended over the beam (Requena-Torres et al. 2006; Martín et al. 2008; Rivilla et al. 2018). In all the observations, each frequency setup was repeated shifting the central frequency by 20-100 MHz in order to identify spurious lines or contamination from the image band.

The IRAM 30m observations were performed during three different sessions in 2019: 10-16th of April, 13-19th of August and 11-15th of December. The dual polarization receiver EMIR was used connected to the fast Fourier transform spectrometers (FFTS), which provided a channel width of 200 kHz in the 3 and 2 mm radio windows. The observations with the Yebes 40m radiotelescope were carried out in February 2020: from the 3rd to 9th and from the 15th to 22th. In this case, the Nanocosmos Q-band (7 mm) HEMT receiver was used which enables ultra broad-band observations in two linear polarizations (Tercero et al. 2021). The receiver was connected to 16 FFTS providing a channel width of 38 kHz and an instantaneous bandwidth of 18.5 GHz per polarization, covering the frequency range between 31.3 GHz and 50.6 GHz.

## 3. ANALYSIS AND RESULTS

We used the software MADCUBA<sup>4</sup> (Martín et al. 2019) to perform the data analysis and line identification. The Spectral Line Identification and Modelling (SLIM) tool of MADCUBA uses the spectroscopic data entries from different molecular catalogs, and generates a synthetic spectra based under the assumption of Local Thermodynamic Equilibrium (LTE) conditions, and considering line opacity effects. The fitted parameters used to reproduce the molecular emission are: column density ( $N$ ), excitation temperature ( $T_{\text{ex}}$ ), local standard of rest velocity ( $v_{\text{LSR}}$ ) and full width at half maximum ( $FWHM$ ).

Both  $\text{HC}(\text{O})\text{SH}$  and  $\text{C}_2\text{H}_5\text{SH}$  have two rotamers, associated with the rotation of their respective C-S bond.  $\text{HC}(\text{O})\text{SH}$  has one cis (c- $\text{HC}(\text{O})\text{SH}$ ) and one trans (t- $\text{HC}(\text{O})\text{SH}$ ) rotamer, being the former  $\sim 330 \text{ K}$  higher in energy (Hocking et al. 1976).  $\text{C}_2\text{H}_5\text{SH}$  has two degenerated  $\pm$  gauche isomers (g- $\text{C}_2\text{H}_5\text{SH}$ ) and one antiperiplanar.

For our analysis we have used the following spectroscopic entries from the CDMS<sup>5</sup> catalog: entries 062515/062516 for trans/cis isomers of  $\text{HC}(\text{O})\text{SH}$  (Hocking et al. 1976), 062523/062524 for gauche/anti isomers of  $\text{C}_2\text{H}_5\text{SH}$  (Kolesníková et al. 2014; Müller et al. 2016), and 048510 for  $\text{CH}_3\text{SH}$  (Xu et al. 2012; Zakharenko et al. 2019).

<sup>2</sup> These are usually referred as carbon-based molecules that have 6 or more atoms (Herbst & Van Dishoeck 2009).

<sup>3</sup> Yebes Observatory is operated by the Spanish Geographic Institute (IGN, Ministerio de Transportes, Movilidad y Agencia Urbana)

<sup>4</sup> Madrid Data CUBe Analysis is a software developed at the Center of Astrobiology in Madrid: <https://cab.inta-csic.es/madcuba/Portada.html>

<sup>5</sup> Cologne Database for Molecular Spectroscopy (Endres et al. 2016). <https://cdms.astro.uni-koeln.de/classic/>

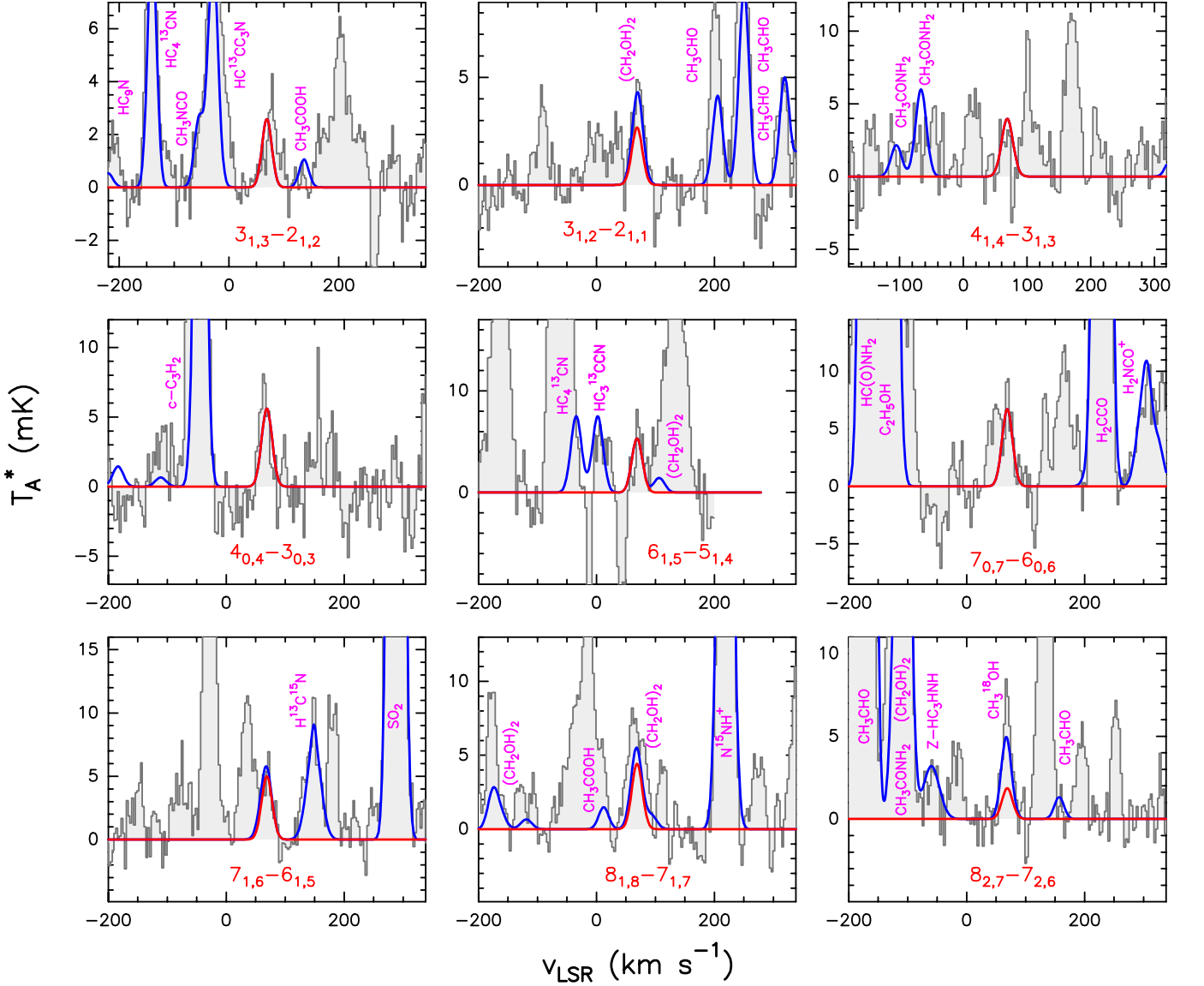


**Figure 1.** Cleanest and brightest lines of *t*-HC(O)SH detected toward G+0.693 labeled with their corresponding quantum numbers in red. The red line shows the best LTE fit to the observed spectra (represented by the black lines). The data has been smoothed up to  $3 \text{ km s}^{-1}$  for an optimal line visualization. The blue lines show the spectra including the emission of all the molecules searched toward G+0.693. Note that these lines are tagged with their corresponding molecular compound in pink.

### 3.1. Detection of *t*-HC(O)SH

The fitting procedure was performed considering the total emission of any other identified molecule in the spectral survey. This evaluation was carried out introducing all the compounds already detected in the ISM and in G+0.693 (see Requena-Torres et al. 2006, 2008; Zeng et al. 2018; Rivilla et al. 2019; Jiménez-Serra et al. 2020). For the analysis, it was also assumed a cosmic microwave background temperature ( $T_{\text{bg}}$ ) of 2.73 K and no background continuum source (Zeng et al. 2020).

The global fit of all rotational lines to the observed data is shown in blue lines in Figure 1, while in red we show the fit of the individual lines of *t*-HC(O)SH, and the observational data in black. As shown in both Figure 1 and Table 1, we have detected a total of nine a-type transitions in the 7 mm and 3 mm bands, each one of them detected above the  $5\sigma$  level in integrated intensity. Note that the SLIM synthetic spectrum shows small deviations with respect to the observations. These deviations are larger than the ones obtained for CH<sub>3</sub>SH and *g*-C<sub>2</sub>H<sub>5</sub>SH (Appendix A). This is due to the fact that the *t*-HC(O)SH lines are significantly weaker than those of CH<sub>3</sub>SH and *g*-C<sub>2</sub>H<sub>5</sub>SH (3-7 mK versus

**Table 1.** Lines of t-HC(O)SH detected toward G+0.693 with their corresponding quantum numbers (QNs), logarithm of the Einstein coefficients ( $\log A_{ul}$ ), degeneracy ( $g_u$ ) and energy ( $E_u$ ) of the upper state. The integrated signal ( $\int T_A^* d\nu$ ) and root mean square (rms) noise level are also provided and used to calculate the signal to noise ratio (SNR) of the detections.

Rest frequency (MHz)	QNs <sup>a</sup>	$g_u$	$E_u$ (K)	$\log A_{ul}$ (s <sup>-1</sup> )	rms (mK)	$\int T_A^* d\nu^b$ (mK km s <sup>-1</sup> )	SNR <sup>c</sup>	Comments
34248.82	3 <sub>1,3</sub> → 2 <sub>1,2</sub>	7	4.3	-6.4784	1.4	56	7.3	clean transition
35915.48	3 <sub>1,2</sub> → 2 <sub>1,1</sub>	7	4.4	-6.4164	1.4	58	7.6	blended with HOCH <sub>2</sub> CH <sub>2</sub> OH
45659.99	4 <sub>1,4</sub> → 3 <sub>1,3</sub>	7	6.0	-6.0647	2.4	88	13.4	clean transition
46737.73	4 <sub>0,4</sub> → 3 <sub>0,3</sub>	7	3.4	-6.0064	2.6	122	8.6	clean transition
71800.18	6 <sub>1,5</sub> → 5 <sub>1,4</sub>	13	11.3	-5.4428	3.5	121	6.3	clean transition
81630.08	7 <sub>0,7</sub> → 6 <sub>0,6</sub>	15	11.8	-5.2587	3.4	153	8.2	slightly blended with CH <sub>3</sub> CH <sub>2</sub> CHO
83749.29	7 <sub>1,6</sub> → 6 <sub>1,5</sub>	15	14.8	-5.2342	3.4	116	11.8	slightly blended with CH <sub>3</sub> COOH
91251.84	8 <sub>1,8</sub> → 7 <sub>1,7</sub>	17	18.1	-5.1166	1.7	104	11.2	slightly blended with (CH <sub>2</sub> OH) <sub>2</sub> and unidentified species
93505.09	8 <sub>2,7</sub> → 7 <sub>2,6</sub>	17	26.5	-5.1061	1.4	46	6.0	blended with CH <sub>3</sub> <sup>18</sup> OH

<sup>a</sup>  $J''_{K_a''K_c''} \rightarrow J'_{K_a'K_c'}$  (where the double prime indicates the upper state).

<sup>c</sup> Signal to noise ratio is calculated from the integrated signal and noise level  $\sigma = \text{rms} \sqrt{\delta v \text{FWHM}}$ , where  $\delta v$  is the velocity resolution of the spectra.

5-12 mK and >40 mK, respectively). However, the fit of all clean t-HC(O)SH lines is consistent with the noise. We also note that for the three slightly blended lines of t-HC(O)SH, the contribution of the other molecules is less than 10% of the total intensity. Despite that the remaining two appear blended, the predicted LTE intensities are consistent with the observed lines. Note that the rest of the t-HC(O)SH lines covered within the observed frequency range are not shown due to strong blending issues.

The physical parameters obtained from the fit are listed in Table 2. The values obtained for  $T_{\text{ex}}$  and  $FWHM$  are consistent with those obtained previously for other molecular species toward this cloud ( $T_{\text{ex}} \sim 5 - 20$  K and linewidths around 20 km s<sup>-1</sup>; Zeng et al. 2018; Rivilla et al. 2020). The low  $T_{\text{ex}}$  indicates that the emission of the molecules in G+0.693 is sub-thermally excited as a result of the low H<sub>2</sub> densities of this source ( $T_{\text{kin}} \sim 150$  K; Requena-Torres et al. 2006; Zeng et al. 2018).

For t-HC(O)SH, the fitted column density gives  $(1.6 \pm 0.1) \times 10^{13}$  cm<sup>-2</sup>. In addition, we derived a  $3\sigma$  upper limit of  $\leq 3 \times 10^{12}$  cm<sup>-2</sup> for c-HC(O)SH (Table 2), as no clear transition has been detected within our dataset. For the calculation, we have assumed the same  $T_{\text{ex}}$ ,  $v_{\text{LSR}}$  and  $FWHM$  as for t-HC(O)SH. A ratio c-HC(O)SH / t-HC(O)SH  $\leq 0.2$  was obtained.

### 3.2. Detection of g-C<sub>2</sub>H<sub>5</sub>SH and CH<sub>3</sub>SH

This molecule was tentatively detected in Orion KL (Kolesníková et al. 2014), based on a few isolated transitions assigned to this isomer. We report here an unambiguous detection of this isomer that confirms its presence in the ISM. We have listed in Table 4 (Appendix A) the transitions measured toward G+0.693. Note that eight of the targeted lines are totally clean (Figure 3, Appendix A) and above the  $5\sigma$  level in integrated intensity. We derived a total column density of  $(4 \pm 2) \times 10^{13}$  cm<sup>-2</sup> (Table 2).

In the case of CH<sub>3</sub>SH, the fit was carried out separating the targeted lines into its  $K_a = 0$  and  $K_a = 1$  levels<sup>6</sup>. The brightest transitions fall into the 3 mm and 2 mm bands as presented in Figure 4 and Table 5 (Appendix B). Note that the agreement between the predicted and observed spectra is excellent for all clean transitions. The column density using the  $K_a = 0$  and  $K_a = 1$  levels is  $(6.5 \pm 0.2) \times 10^{14}$  cm<sup>-2</sup> (Table 2). This gives a ratio of CH<sub>3</sub>SH / g-C<sub>2</sub>H<sub>5</sub>SH =  $16 \pm 7$ . Note that the column density of  $K_a = 2$  and remaining transitions in CH<sub>3</sub>SH contribute less than a 10% in the total determined.

<sup>6</sup> The moments of inertia of CH<sub>3</sub>SH frame it in the limiting prolate case,  $\kappa = (2B - A - C)/(A - C) \approx -0.988$ .

**Table 2.** Physical parameters of the species derived by LTE analysis in MADCUBA.

Molecular formula	N ( $\times 10^{13} \text{ cm}^{-2}$ )	T <sub>ex</sub> (K)	v <sub>LSR</sub> ( $\text{km s}^{-1}$ )	FWHM ( $\text{km s}^{-1}$ )	Abundance ( $\frac{N(X)}{N(H_2)} \times 10^{-10}$ )
<b>trans – HC(O)SH</b>	$1.6 \pm 0.1$	$10 \pm 1$	69.0 <sup>a</sup>	21.0 <sup>a</sup>	$1.2 \pm 0.2$
<b>cis – HC(O)SH</b>	$\leq 0.3$	10.0	69.0 <sup>a</sup>	21.0 <sup>a</sup>	$\leq 0.2$
<b>g – C<sub>2</sub>H<sub>5</sub>SH</b>	$4 \pm 2$	$10 \pm 5$	69.0 <sup>a</sup>	20.0 <sup>a</sup>	$3 \pm 1$
<b>a – C<sub>2</sub>H<sub>5</sub>SH</b>	$\leq 2.3$	9.91	69.0 <sup>a</sup>	20.0 <sup>a</sup>	$\leq 1.7$
CH <sub>3</sub> SH, K <sub>a</sub> = 0	$46.8 \pm 0.5$	$8.5 \pm 0.1$	$68.0 \pm 0.1$	$21.2 \pm 0.3$	-
CH <sub>3</sub> SH, K <sub>a</sub> = 1	$18.6 \pm 0.7$	$14.9 \pm 0.5$	$68.8 \pm 0.3$	$22.0 \pm 0.7$	-
<b>CH<sub>3</sub>SH</b>	$65 \pm 2$	-	-	-	$48 \pm 5$
<b>t – HCOOH</b>	$20 \pm 4$	$10 \pm 2$	$68 \pm 2$	$22 \pm 5$	$15 \pm 4$

<sup>a</sup>Value fixed in the fit.

Finally, we note that both <sup>13</sup>C and <sup>34</sup>S isotopologues of CH<sub>3</sub>SH have also been detected with a few clean lines and will be presented in a forthcoming paper (Colzi et al. in prep.).

### 3.3. Molecular Abundances and comparison with their O-bearing analogues

To derive the fractional abundances of these species relative to H<sub>2</sub>, we have assumed an H<sub>2</sub> column density of  $N_{H_2} = 1.35 \times 10^{23} \text{ cm}^{-2}$  (Martín et al. 2008). This gives  $\sim 3 \times 10^{-10}$ ,  $\sim 1 \times 10^{-10}$  and  $\sim 5 \times 10^{-9}$  for g-C<sub>2</sub>H<sub>5</sub>SH, t-HC(O)SH and CH<sub>3</sub>SH, respectively (Table 2).

In Figure 2 we have plotted these values and compared them with the abundances obtained for their OH molecular analogues, namely: C<sub>2</sub>H<sub>5</sub>OH (ethanol), HC(O)OH (formic acid) and CH<sub>3</sub>OH (methanol). We obtained a ratio CH<sub>3</sub>OH / CH<sub>3</sub>SH = 23, C<sub>2</sub>H<sub>5</sub>OH / C<sub>2</sub>H<sub>5</sub>SH = 15 and HC(O)OH / HC(O)SH = 13. Although these OH-analogues are more abundant by a factor  $\geq 10$ , the resulting trend is strikingly similar. Note, however, that this trend is lost when we compare molecules such as carbon monosulfide (CS) and thioformaldehyde (H<sub>2</sub>CS) with their O-bearing analogues, resulting in H<sub>2</sub>CO / H<sub>2</sub>CS = 3.5 and CO / CS =  $3.5 \times 10^3$  (Figure 2).

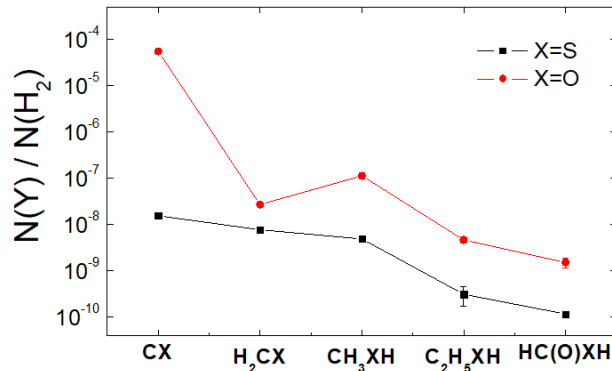


**Figure 2.** Molecular abundances wrt H<sub>2</sub> for the reported detections and their OH-analogues (CH<sub>3</sub>OH, C<sub>2</sub>H<sub>5</sub>OH and HC(O)OH) including CS, CO, H<sub>2</sub>CO and H<sub>2</sub>CS. The lines that connect each dot do not have any physical meaning but are just a visual aid.

Since CH<sub>3</sub>OH, C<sub>2</sub>H<sub>5</sub>OH, H<sub>2</sub>CO, CO and CS are optically thick toward G+0.693, the column density of these molecules were inferred from CH<sub>3</sub><sup>18</sup>OH, <sup>13</sup>CH<sub>3</sub>CH<sub>2</sub>OH, H<sub>2</sub>C<sup>18</sup>O, C<sup>18</sup>O and <sup>13</sup>C<sup>34</sup>S. It was assumed <sup>16</sup>O / <sup>18</sup>O = 250 and <sup>12</sup>C / <sup>13</sup>C = 21 (Armijos-Abendaño et al. 2015) and <sup>32</sup>S / <sup>34</sup>S = 22 (Wilson et al. 1999). For HC(O)OH, the main isotopologue of HC(O)OH was employed as the ratio H<sup>12</sup>C(O)OH / H<sup>13</sup>C(O)OH is consistent with the <sup>12</sup>C / <sup>13</sup>C ratio. For the sulfur-analogues, except CS, we do not expect opacity issues due to their much lower abundances.

The information about the fit employed for the molecules presented in Figure 2 or their isotopologues is included in Appendix B.

## 4. DISCUSSION

### 4.1. Comparison with previous observations

We have compared different column density ratios obtained between the S-bearing compounds measured toward G+0.693 and two other sources, namely: Orion KL (Kolesniková et al. 2014) and Sgr B2(N2) (Müller et al. 2016, see Table 3).

From this table, we find that all abundance ratios measured in G+0.693 are strikingly similar. For instance, when we compare SH-bearing molecules with their OH-analogues ( $\text{CH}_3\text{OH} / \text{CH}_3\text{SH}$  and  $\text{C}_2\text{H}_5\text{OH} / \text{C}_2\text{H}_5\text{SH}$ ) we recover the trend already found in Figure 2, which might indicate a similar chemistry between OH- and SH-bearing species. The  $\text{CH}_3\text{OH} / \text{CH}_3\text{SH}$  ratio measured in G+0.693 is a factor of 5 lower than those found in Sgr B2(N2) and Orion KL, which indicates that G+0.693 is richer in sulfur-bearing species than the two massive hot cores. This may be related to the fact that the chemistry of this cloud is affected by large-scale shocks (Requena-Torres et al. 2006; Zeng et al. 2018). Since sulfur is heavily depleted on grains (possibly in the form of  $\text{S}_8$  and other sulfur allotropes; Shingledecker et al. 2020), the sputtering of dust grains induced by shocks could liberate a significant fraction of the locked sulfur.

The  $\text{C}_2\text{H}_5\text{OH} / \text{C}_2\text{H}_5\text{SH}$  ratio is comparable to the value determined toward Orion KL while there is a difference by a factor of 10 between G+0.693 and the upper limit toward Sgr B2(N2). All these ratios suggest that sulfur is less incorporated into molecules than oxygen, which again might be due to the fact that a significant fraction of sulfur is locked up in grains.

**Table 3.** Relative abundances of molecules and comparison with other sources.

Source	$\text{CH}_3\text{SH} / \text{C}_2\text{H}_5\text{SH}$	$\text{CH}_3\text{OH} / \text{C}_2\text{H}_5\text{OH}$	$\text{CH}_3\text{OH} / \text{CH}_3\text{SH}$	$\text{C}_2\text{H}_5\text{OH} / \text{C}_2\text{H}_5\text{SH}$
G+0.693	$16 \pm 7$	$24 \pm 4^{c,d}$	$23 \pm 3^c$	$15 \pm 7^d$
Sgr B2(N2) <sup>a</sup>	$\geq 21$	20	118	$\geq 125$
Orion KL <sup>b</sup>	5	31	120	20

<sup>a</sup>Data taken from Müller et al. (2016).

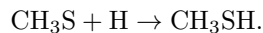
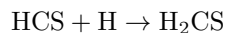
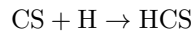
<sup>b</sup>Data taken from Kolesniková et al. (2014).

<sup>c</sup>Data inferred from  $\text{CH}_3^{18}\text{OH}$  assuming  $^{16}\text{O} / ^{18}\text{O} = 250$  (Armijos-Abendaño et al. 2015).

<sup>d</sup>Data inferred from  $^{13}\text{CH}_3\text{CH}_2\text{OH}$  assuming  $^{12}\text{C} / ^{13}\text{C} = 21$  (Armijos-Abendaño et al. 2015).

### 4.2. Interstellar chemistry of thiols

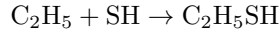
In order to understand the chemistry of S-bearing compounds, different models have been proposed based on the simple molecules detected in the gas phase (Müller et al. 2016; Gorai et al. 2017; Lamberts 2018; Laas et al. 2019).  $\text{CH}_3\text{SH}$  is thought to be formed on grain surfaces by sequential hydrogenations starting from CS:



The last step could also yield other products but theoretical calculations show a branching ratio (br) of  $\sim 75\%$  for  $\text{CH}_3\text{SH}$  (Lamberts 2018). This is a viable mechanism since approximately half of the CS present in the ices is available to undergo hydrogenation, while the other half is converted to OCS (Palumbo et al. 1997). Once formed,

CH<sub>3</sub>SH could remain stored in the ices until released by grain sputtering in the large-scale shocks present in G+0.693 (Requena-Torres et al. 2006; Zeng et al. 2020).

Likewise, ethyl mercaptan is proposed to be formed by radical-radical reactions (Gorai et al. 2017; Müller et al. 2016) such as:



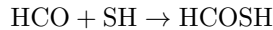
Observations of the reactants could give us a hint of the dominant reaction based on the measured column densities. However, chemical modeling is needed to understand the efficiency of these formation routes. Note that CH<sub>2</sub>SH is the main product of the hydrogenation of H<sub>2</sub>CS (Lamberts 2018).

To our knowledge, there is no information available in the literature about the chemistry of HC(O)SH. However, we can make a guess and assume similar astrochemical pathways for the SH-based species as the ones for their OH-analogues. A possible pathway to HC(O)SH could mimic the formation of HC(O)OH. Ioppolo et al. (2011) showed that the formation of HC(O)OH starts from CO and the OH radical in the ice. The thiol-equivalent reaction would be:

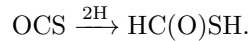


The first step has been found to be efficient by Adriaens et al. (2010), but further experimental and/or theoretical work is needed to investigate whether HSCO could be hydrogenated further.

Another possibility could be:



or



The first reaction was initially proposed for HC(O)OH by Garrod & Herbst (2006) and could be a viable mechanism since SH can be formed on surfaces from S + H or H + H<sub>2</sub>S via tunneling (Vidal et al. 2017). The second involves the sequential hydrogenation of OCS, which is a molecule detected in ices (Palumbo et al. 1997) and it is moderately abundant in the gas phase in G+0.693 (N > 10<sup>15</sup> cm<sup>-2</sup>; Armijos-Abendaño et al. 2015). Theoretical studies about these chemical networks are currently under work and will be presented in a forthcoming paper (Molpeceres et al. in prep).

#### 4.3. Implications for theories on the origin of life

As it was previously stated, thioacids and thioesters have been proposed as key agents in the polymerization of amino acids into peptides and proteins (Foden et al. 2020; Muchowska et al. 2020). In some of these works, it is stressed the importance of cystein, HSCH<sub>2</sub>CH(NH<sub>2</sub>)COOH, as the primary organic source of sulfide in biology and a key catalyst in the abiotic polymerization of peptides. Smaller thiols such as CH<sub>3</sub>SH and C<sub>2</sub>H<sub>5</sub>SH are also believed to play a key role in prebiotic chemistry and in theories about the origin of life, since they are precursors for the synthesis of the aminoacids methionine and ethionine (Parker et al. 2011). In turn, HC(O)SH could be an important ingredient in the phosphorylation of nucleosides as demonstrated by Lohrmann et al. (1968).

The idea of an extraterrestrial delivery of SH-compounds onto Earth, is supported by the detection of CH<sub>3</sub>SH in Murchinson carbonaceous chondrite (Tingle et al. 1991) and in the coma of the 67P/Churyumov-Gerasimenko comet (Calmonte et al. 2016). In the latter, C<sub>2</sub>H<sub>6</sub>S was also detected (either in the form of C<sub>2</sub>H<sub>5</sub>SH or CH<sub>3</sub>SCH<sub>3</sub> - dimethyl sulfide-) with an abundance ratio CH<sub>3</sub>SH / C<sub>2</sub>H<sub>6</sub>S ~ 10 which is consistent with the value obtained in G+0.693 (Table 3). This resemblance could be possibly indicating a pre-solar origin of these compounds. Still, further studies are required within other regions in the ISM and planetary bodies to make a proper connection.

In summary, not only have our observations confirmed the presence of sulfur-bearing complex organics such as CH<sub>3</sub>SH and C<sub>2</sub>H<sub>5</sub>SH, but they also have revealed the existence of the simplest thioacid known, HC(O)SH, in the ISM.

## 5. ACKNOWLEDGMENTS

L.F.R.-A. acknowledges support from a JAE-intro ICU studentship funded by the Spanish National Research Council (CSIC). L.F.R.-A., V.M.R. and L.C. also acknowledge support from the Comunidad de Madrid through the Atracción de Talento Investigador Modalidad 1 (Doctores con experiencia) Grant (COOL: Cosmic Origins Of Life; 2019-T1/TIC-15379; PI: V.M.Rivilla). I.J.-S. and J.M.-P. have received partial support from the State Research Agency (AEI)

through project numbers PID2019-105552RB-C41 and MDM-2017-0737 Unidad de Excelencia "María de Maeztu" - Centro de Astrobiología (CSIC-INTA). PdV and BT thank the support from the European Research Council through Synergy Grant ERC-2013-SyG, G.A. 610256 (NANOCOSMOS) and from the Spanish Ministerio de Ciencia e Innovación (MICIU) through project PID2019-107115GB-C21. BT also thanks the Spanish MICIU for funding support from grants AYA2016-75066-C2-1-P and PID2019-106235GB-I00.

*Facilities:* IRAM 30m, Yebes 40m

*Software:* MADCUBA

## REFERENCES

- Adriaens D.A., Goumans T.P.M., Catlow C.R.A., et al. 2010, *J. Phys. Chem. C*, 114, 1892.
- Armijos-Abendaño J., Martín-Pintado, J., Requena-Torres M.A. et al. 2015, *MNRAS*, 446, 3842
- Asplund M., Grevesse N., Sauval A. et al. 2009, *ARA&A*, 47
- Calmonte, U., Altwegg K., Balsiger H. et al. 2016, *MNRAS*, 462, S253
- Chandru K., Gilbert A., Butch C., et al. 2016, *Sci. Rep.*, 6, 29883
- Endres C.P., Schlemmer S., Schilke P., et al. 2016, *J. Mol. Spectrosc.*, 327, 95
- Foden C.S., Islam S., Fernández-García C., et al. 2020, *Science*, 370, 865
- Garrod R.T. and Herbst E. 2006, *A&A*, 457, 927
- Gibb E., Nummelin A., Irvine W.M., et al. 2000, *ApJ*, 545, 309
- Gorai P., Das A., Sivaraman B., et al. 2017, *ApJ*, 836, 70
- Herbst E. and E.F. Van Dishoeck, 2009, *ARA&A*, 47, 427
- Hocking W.H. and Winnewisser G., 1976, *Z. Naturforsch.*, 31a, 995
- Ioppolo S., Van Boheemen Y., Cuppen H., et al. 2011, *MNRAS*, 413, 2281
- Jabri A., Tercero B., Margulès, L., et al. 2020, *A&A*, 644, A102
- Jiménez-Escobar, A., Muñoz Caro, G.M. and Chen, Y.J. 2014, *MNRAS*, 443, 343
- Jiménez-Serra I., Martín-Pintado J., Rivilla V.M., et al. 2020, *Astrobiology*, 20, 1048
- Kolesniková L., Tercero B., Cernicharo J. et al. 2014, *ApJL*, 784, L7
- Laas J.C. and Caselli P., 2019, *A&A*, 624, A108
- Lamberts T. 2018, *A&A*, 615, L2
- Leman L.J. and Ghadiri M.R., 2017, *Synlett*, 28, 68
- Linke R., Frerking M.A. and Thaddeus P., 1979, *ApJ*, 234, L139
- Lohrmann R. and Orgel L.E., 1968, *Science*, 161, 64
- Majumdar L., Gratier P., Vidal T., et al. 2016, *MNRAS*, 458, 1859
- Margulès L, Ilyushin V.V., McGuire B.A., et al. 2020, *J. Mol. Spectrosc.*, 371, 111304
- Martín S., Martín-Pintado J., Blanco-Sánchez, C. et al. 2019, *A&A*, 631, A159
- Martín S., Requena-Torres M.A., Martín-Pintado J., et al. 2008, *ApJ*, 678, 245
- Motiyenko R., Belloche A., Garrod R., et al. 2020, *A&A*, 642, A29
- Muchowska K.B. & Moran J. 2020, *Science*, 370, 767-768
- Müller H.S.P., Belloche A., Li-Hong X., et al. 2016, *A&A*, 587, A92
- Palumbo M.E., T.R. Geballe and A.G.G.M. Tielens 1997, *ApJ*, 479, 839
- Parker E.T., Cleaves H.J., Callahan M.P., et al. 2011, *Orig. Life Evol. Biosph.*, 41, 201
- Requena-Torres M.A., Martín-Pintado J., Rodríguez-Fernández N.J. et al. 2006, *A&A*, 455, 971
- Requena-Torres M.A., Martín-Pintado J., Martín S. et al. 2008, *ApJ*, 672, 352
- Rivilla V.M., Martín-Pintado J., Jiménez-Serra I., et al. 2019, *MNRAS*, 483, L114
- Rivilla V.M., Martín-Pintado J., Jiménez-Serra I., et al. 2020, *ApJL*, 899, L28
- Rivilla V.M., Jiménez-Serra I., Zeng S., et al. 2018, *MNRAS*, 475, L30
- Shalayel I., Youssef-Saliba S., Vazart F., et al. 2020, *Eur. J. Org. Chem*, 20, 3019
- Shingledecker C.N., Lamberts T., Laas J.C. et al. 2020, *ApJ*, 888, 52
- Sinclair, M.W., Fourikis, N., Ribes, J.C. et al. 1973, *Aust. J. Phys.*, 26, 85
- Tercero F., López-Pérez J.A., Gallego J.D., et al. 2021, *A&A*, 645, 22
- Tingle N., Becker, C.H. and Ripudaman, M. 1991, *Meteorit. Planet. Sci.*, 26, 117



T.H.G. Vidal, J.-C. Loison, A.Y. Jaziri, et al. 2017,  
MNRAS, 469, 435

Wilson T.L. 1999, Rep. Prog. Phys., 62, 143

Xu L.H., Lees R.M., Grabbe G.T., et al. 2012, JChPh, 137,  
104313

Zakharenko O., Ilyushin V.V., Lewen F., et al. 2019, A&A,  
629, A73

Zeng S., Jiménez-Serra I., Rivilla, V.M., et al. 2018,  
MNRAS, 478, 2962

Zeng S., Zhang Q., Jiménez-Serra I., et al. 2020, MNRAS,  
497, 4896

## APPENDIX

A. DETECTIONS OF  $C_2H_5SH$  AND  $CH_3SH$  IN G+0.693

In Figures 3 and 4 and Tables 4 and 5 the fit of  $g$ - $C_2H_5SH$  and  $CH_3SH$  is shown. The fitting procedure followed has been the same as  $t$ - $HC(O)SH$ , explained in the main text.

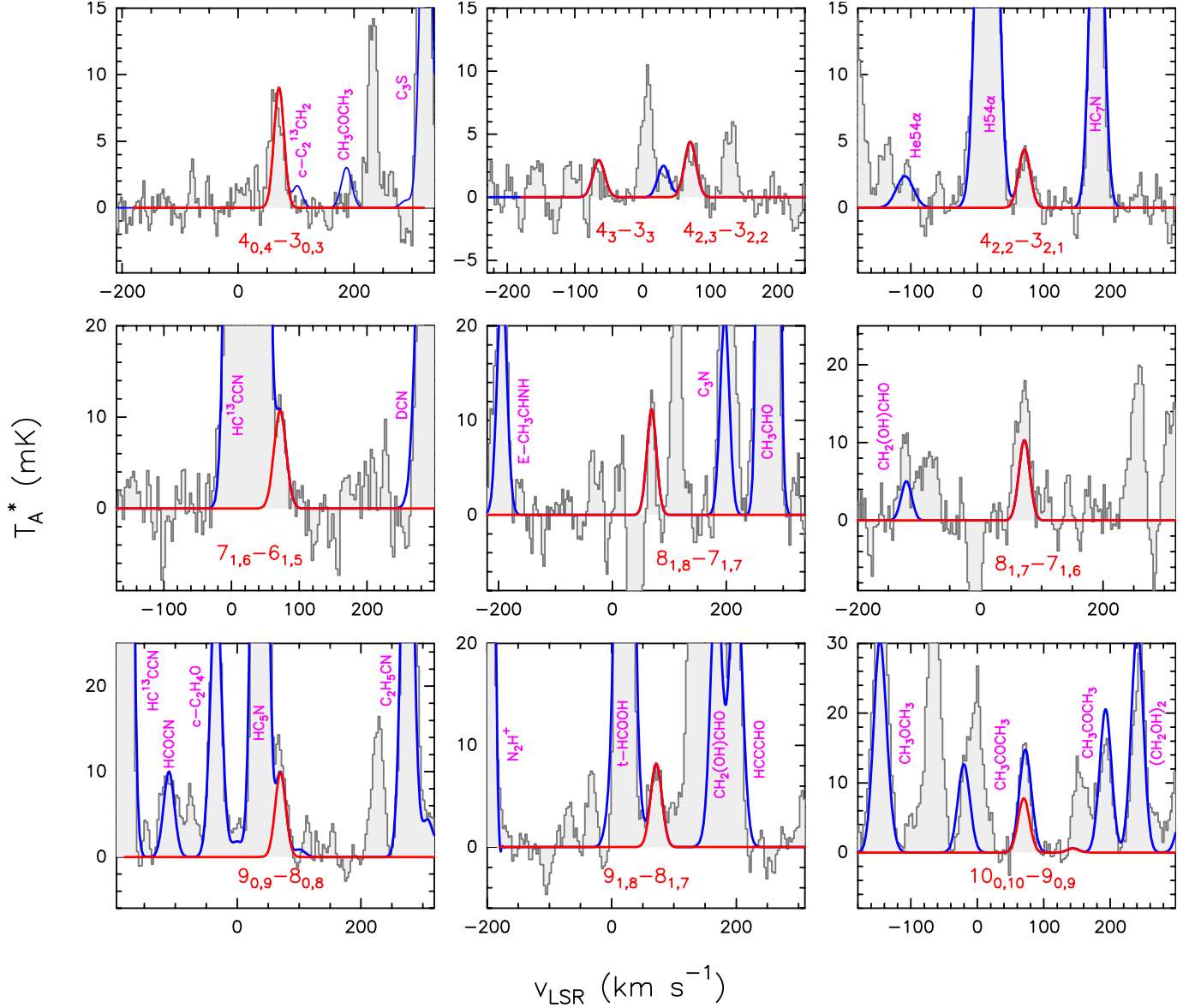


**Figure 3.** Cleanest and brightest lines of  $g$ - $C_2H_5SH$  detected toward G+0.693. The red line shows the best LTE fit to the observed spectra (represented by the black lines) with their corresponding quantum numbers in red ( $J_{K_a, K_c}$ ; see Table 4 for a description of their tunneling states). The data has been smoothed up to  $3 \text{ km s}^{-1}$  for an optimal line visualization. The blue lines show the spectra including the emission of all the molecules searched toward the cloud. Note that these lines are tagged with their corresponding molecular compound in pink.

**Table 4.** Lines of g-C<sub>2</sub>H<sub>5</sub>SH detected toward G+0.693 with their corresponding QNs and tunneling states (TS), log A<sub>ul</sub>, g<sub>u</sub> and E<sub>u</sub>.  $\int T_A^* d\nu$  and rms are also provided and used to calculate the SNR of the detected lines.

Rest frequency (MHz)	QNs	TS $\nu'' \rightarrow \nu'$	g <sub>u</sub>	E <sub>u</sub> (K)	log A <sub>ul</sub> (s <sup>-1</sup> )	rms (mK)	$\int T_A^* d\nu$ (mK km s <sup>-1</sup> )	SNR	Comments
40499.173	4 <sub>0,4</sub> → 3 <sub>0,3</sub>	1 → 1	9	3.0	-6.1161	1.4	225	29	clean transition <sup>a</sup>
40499.591	4 <sub>0,4</sub> → 3 <sub>0,3</sub>	0 → 0	9	2.9	-6.1163	1.4	-	-	-
40558.849	4 <sub>2,3</sub> → 3 <sub>2,2</sub>	1 → 1	9	7.6	-6.2391	1.2	107	16	clean transition <sup>a</sup>
40559.284	4 <sub>2,3</sub> → 3 <sub>2,2</sub>	0 → 0	9	7.5	-6.2392	1.2	-	-	-
40576.963	4 <sub>3,2</sub> → 3 <sub>3,1</sub>	1 → 1	9	13.2	-6.2004	1.2	72	11	clean transition <sup>a</sup>
40577.299	4 <sub>3,1</sub> → 3 <sub>3,0</sub>	1 → 1	9	13.2	-6.2004	1.2	-	-	-
40577.432	4 <sub>3,2</sub> → 3 <sub>3,1</sub>	0 → 0	9	13.2	-6.2004	1.2	-	-	-
40577.769	4 <sub>3,1</sub> → 3 <sub>3,0</sub>	0 → 0	9	13.2	-6.2004	1.2	-	-	-
40622.316	4 <sub>2,2</sub> → 3 <sub>2,1</sub>	1 → 1	9	7.6	-6.2370	1.2	107	16	clean transition <sup>a</sup>
40622.792	4 <sub>2,2</sub> → 3 <sub>2,1</sub>	0 → 0	9	7.5	-6.2371	1.2	-	-	-
72466.861	7 <sub>1,6</sub> → 6 <sub>1,5</sub>	1 → 1	15	11.7	-5.3458	2.8	261	17	clean transition <sup>a</sup>
72468.152	7 <sub>1,6</sub> → 6 <sub>1,5</sub>	0 → 0	15	11.6	-5.3459	2.8	-	-	-
79204.501	8 <sub>1,8</sub> → 7 <sub>1,7</sub>	1 → 1	17	14.6	-5.2243	1.8	204	24	clean transition <sup>a</sup>
79204.501	8 <sub>1,8</sub> → 7 <sub>1,7</sub>	0 → 0	17	14.6	-5.2243	1.8	-	-	-
82782.441	8 <sub>1,7</sub> → 7 <sub>1,6</sub>	1 → 1	17	15.2	-5.1667	1.8	233	30	slightly blended with unidentified line <sup>a</sup>
82783.912	8 <sub>1,7</sub> → 7 <sub>1,6</sub>	0 → 0	17	15.1	-5.1668	1.4	-	-	-
90516.341	9 <sub>0,9</sub> → 8 <sub>0,8</sub>	1 → 1	19	17.6	-5.0412	1.2	223	34	slightly blended with unidentified line <sup>a</sup>
90516.926	9 <sub>0,9</sub> → 8 <sub>0,8</sub>	0 → 0	19	17.5	-5.0414	1.2	-	-	-
93082.083	9 <sub>1,8</sub> → 8 <sub>1,7</sub>	1 → 1	19	19.1	-5.0096	2.0	191	18	clean transition <sup>a</sup>
93083.720	9 <sub>1,8</sub> → 8 <sub>1,7</sub>	0 → 0	19	19.1	-5.0097	2.0	-	-	-
100391.240	10 <sub>0,10</sub> → 9 <sub>0,9</sub>	1 → 1	21	21.9	-4.9042	1.8	171	17	blended with CH <sub>3</sub> COCH <sub>3</sub> <sup>a</sup>
100391.791	10 <sub>0,10</sub> → 9 <sub>0,9</sub>	0 → 0	21	21.8	-4.9042	1.8	-	-	-

<sup>a</sup>In these cases, the lines are composed by a blend of individual g-C<sub>2</sub>H<sub>5</sub>SH lines. Here, SNR is calculated according with Figure 3.

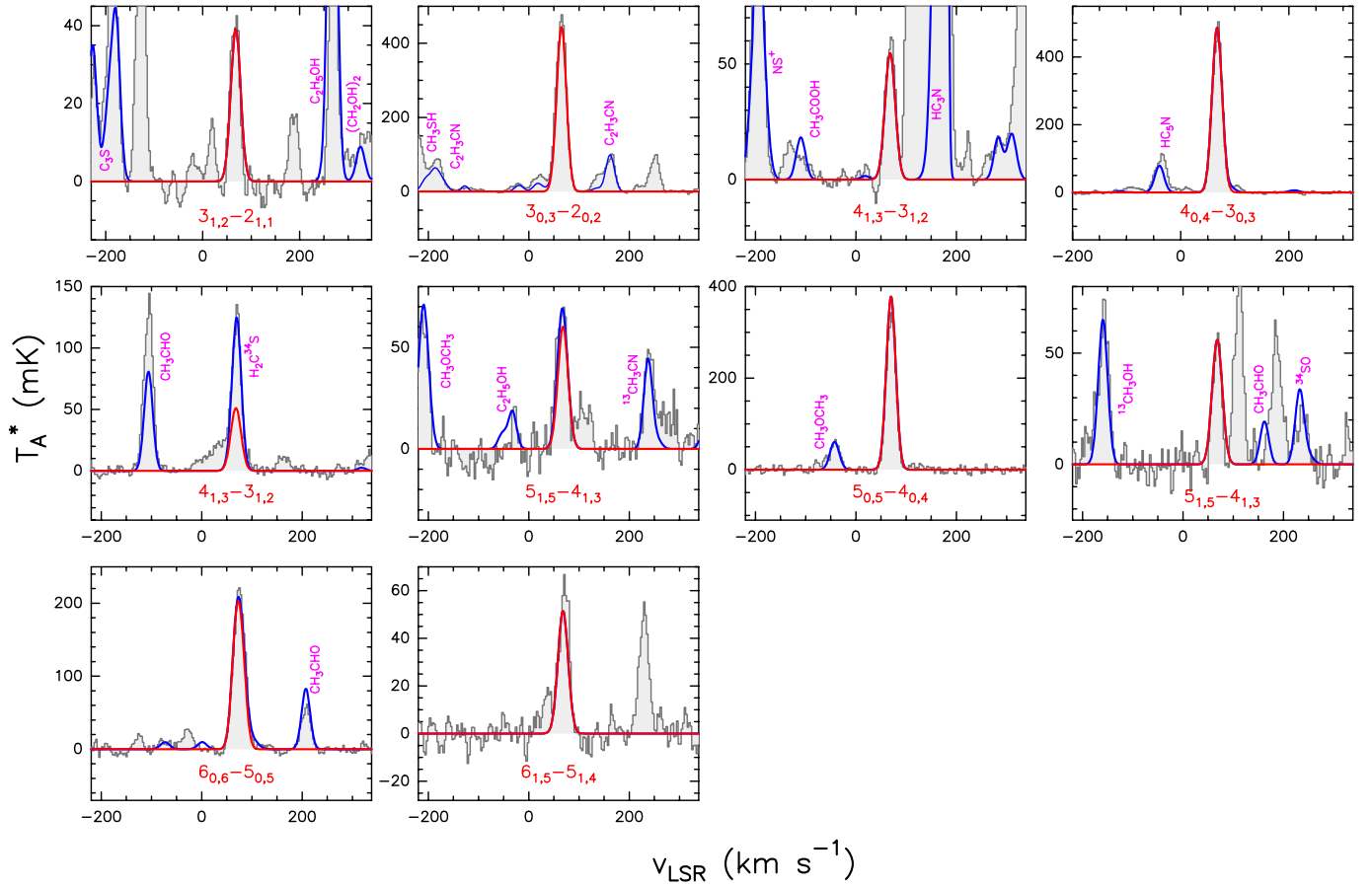


**Figure 4.** Cleanest and brightest lines of  $\text{CH}_3\text{SH}$  detected toward G+0.693. The red line shows the best LTE fit to the observed spectra (represented by the black lines) with their corresponding quantum numbers in red ( $J_{K_a, K_c}$ ; see Table 5 for the description of their torsional states). The data has been smoothed up to  $3 \text{ km s}^{-1}$  for an optimal line visualization. The blue lines show the spectra including the emission of all the molecules searched toward the cloud. Note that these lines are tagged with their corresponding molecular compound in pink.

**Table 5.** Lines of CH<sub>3</sub>SH detected toward G+0.693 with their corresponding quantum numbers (QNs) and torsional symmetry (T<sub>s</sub>), logarithm of the Einstein coefficients (log A<sub>ul</sub>), degeneracy (g<sub>u</sub>) and energy (E<sub>u</sub>) of the upper state. The peak intensity (I<sub>peak</sub>) and root mean square (rms) noise level are also provided and used to calculate the signal to noise ratio (SNR) of the detected lines.

Rest frequency (MHz)	QNs	T <sub>s</sub>	g <sub>u</sub>	E <sub>u</sub> (K)	log A <sub>ul</sub> (s <sup>-1</sup> )	rms (mK)	I <sub>peak</sub> (mK)	SNR	Comments
75085.898	3 <sub>1,2</sub> → 2 <sub>1,1</sub>	A <sup>+</sup>	7	8.7	-5.5086	2.7	39	14	clean transition
75862.889	3 <sub>0,3</sub> → 2 <sub>0,2</sub>	A <sup>+</sup>	7	3.6	-5.4444	2.3	260	113	clean transition
75864.422	3 <sub>0,3</sub> → 2 <sub>0,2</sub>	E	7	5.1	-5.4443	2.3	221	96	clean transition
100110.219	4 <sub>1,3</sub> → 3 <sub>1,2</sub>	A <sup>+</sup>	9	12.3	-5.0966	3.1	55	18	clean transition
101139.150	4 <sub>0,4</sub> → 3 <sub>0,3</sub>	A <sup>+</sup>	9	7.3	-5.0554	2.9	271	93	clean transition
101139.655	4 <sub>0,4</sub> → 3 <sub>0,3</sub>	E	9	8.7	-5.0543	2.9	230	79	clean transition
101284.366	4 <sub>1,3</sub> → 3 <sub>1,2</sub>	E	9	13.5	-5.0818	2.9	51	18	blended with H <sub>2</sub> C <sup>34</sup> S
125130.863	5 <sub>1,5</sub> → 4 <sub>1,3</sub>	A <sup>+</sup>	11	17.1	-4.7869	6.2	61	10	slightly blended with HC <sub>5</sub> N
126403.834	5 <sub>0,5</sub> → 4 <sub>0,4</sub>	E	11	13.6	-4.7556	6.4	183	29	clean transition
126405.676	5 <sub>0,5</sub> → 4 <sub>0,4</sub>	A <sup>+</sup>	11	12.2	-4.7556	6.4	215	34	clean transition
126683.419	5 <sub>1,5</sub> → 4 <sub>1,9</sub>	A <sup>+</sup>	11	18.4	-4.7707	6.5	56	9	clean transition
151654.218	6 <sub>0,6</sub> → 5 <sub>0,5</sub>	E	13	19.6	-4.5123	5.4	116	22	clean transition
151660.047	6 <sub>0,6</sub> → 5 <sub>0,5</sub>	A <sup>+</sup>	13	18.2	-4.5123	5.4	136	25	clean transition
152129.018	6 <sub>1,5</sub> → 5 <sub>1,4</sub>	E	13	24.4	-4.5210	4.5	52	12	clean transition

B. FIGURES AND TABLES OF  $^{13}\text{C}^{34}\text{S}$ ,  $\text{H}_2\text{CS}$ ,  $\text{H}_2\text{C}^{18}\text{O}$ ,  $\text{CH}_3^{18}\text{OH}$ ,  $^{13}\text{CH}_3\text{CH}_2\text{OH}$ 

We show a few intense the lines selected within the targeted frequency coverage in G+0.693 for some of the species used in the molecular abundances calculations in Figure 2. Note that other visible lines not shown in these figures or tables are either heavily blended or in a bad part of the spectra.

**Table 6.** Lines of  $^{13}\text{C}^{34}\text{S}$  detected toward G+0.693 with their corresponding spectroscopic information and parameters derived from the LTE fit.

Rest frequency (MHz)	QNs	$g_u$	$E_u$ (K)	$\log A_{ul}$ ( $\text{s}^{-1}$ )	rms (mK)	$\int T_A^* d\nu$ (mK km s $^{-1}$ )	SNR	Comments
45463.424	1 $\rightarrow$ 0	3	0.0	-5.8546	2.0	364	> 20	clean transition
90926.026	2 $\rightarrow$ 1	5	2.0	-4.8723	2.5	854	> 20	clean transition
136387.028	3 $\rightarrow$ 2	7	6.6	-4.3141	2.1	796	> 20	clean transition

**Table 7.** Lines of  $\text{H}_2\text{CS}$  detected toward G+0.693 with  $I_{\text{peak}} > 0.8\text{K}$  and their corresponding spectroscopic information and parameters derived from the LTE fit.

Rest frequency (MHz)	QNs	$g_u$	$E_u$ (K)	$\log A_{ul}$ ( $\text{s}^{-1}$ )	rms (mK)	$I_{\text{peak}}$ (K)	SNR	Comments
101477.8048	3 $_{1,3} \rightarrow$ 2 $_{1,2}$	21	2.0	-4.8996	2.9	1.213	> 20	clean transition
103040.447	3 $_{0,3} \rightarrow$ 2 $_{0,2}$	7	5.0	-4.8285	2.6	0.951	> 20	clean transition
104617.027	3 $_{1,2} \rightarrow$ 2 $_{1,1}$	27	18.2	-4.8599	2.1	1.169	> 20	clean transition
135298.26	4 $_{1,4} \rightarrow$ 3 $_{1,3}$	27	22.9	-4.4859	7.0	1.213	> 20	clean transition
137371.21	4 $_{0,4} \rightarrow$ 3 $_{0,3}$	9	9.9	-4.438	3.1	0.823	> 20	clean transition
139483.68	4 $_{1,3} \rightarrow$ 3 $_{1,2}$	27	23.2	-4.4462	2.7	1.197	> 20	clean transition

**Table 8.** Lines of  $\text{H}_2\text{C}^{18}\text{O}$  detected toward G+0.693 with their corresponding spectroscopic information and parameters derived from the LTE fit.

Rest frequency (MHz)	QNs	$g_u$	$E_u$ (K)	$\log A_{ul}$ ( $\text{s}^{-1}$ )	rms (mK)	$\int T_A^* d\nu$ (mK km s $^{-1}$ )	SNR	Comments
134435.920	2 $_{1,2} \rightarrow$ 1 $_{1,1}$	15	2.0	-4.3361	6.7	839	> 20	slightly blended with $\text{CH}_3\text{CHO}$
138770.86	2 $_{0,2} \rightarrow$ 1 $_{0,1}$	5	3.3	-4.1697	2.7	814	> 20	clean transition
143213.07	2 $_{1,1} \rightarrow$ 1 $_{1,0}$	15	15.3	-4.2536	2.1	824	> 20	clean transition

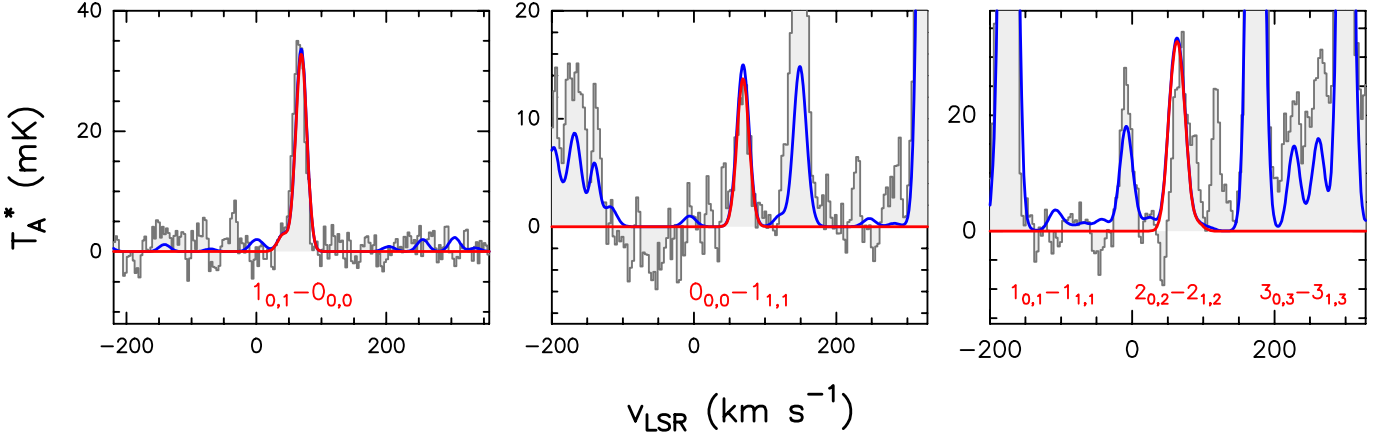


**Figure 5.** Selected lines of CH<sub>3</sub><sup>18</sup>OH detected toward G+0.693. Black, red and blue lines represent the observational data, the individual lines of CH<sub>3</sub><sup>18</sup>OH and the global fit considering all the species detected, respectively. See Table 9 for a complete description of their quantum numbers.

**Table 9.** Lines of CH<sub>3</sub><sup>18</sup>OH detected toward G+0.693 with their corresponding spectroscopic information and parameters derived from the LTE fit.

Rest frequency (MHz)	QNs	T <sub>s</sub>	g <sub>u</sub>	E <sub>u</sub> (K)	log A <sub>ul</sub> (s <sup>-1</sup> )	rms (mK)	∫ T <sub>A</sub> * dν (mK km s <sup>-1</sup> )	SNR	Comments
46364.313	1 <sub>0,1</sub> → 0 <sub>0,0</sub>	A	12	0.0	-4.8985	2.8	709	> 20	clean transition
93505.902	2 <sub>1,1</sub> → 1 <sub>1,0</sub>	A	20	16.6	-5.6353	1.9	68	7	blended with t-HC(O)SH
150698.06	1 <sub>0,1</sub> → 1 <sub>1,1</sub>	E	12	7.8	-4.7223	3.1	466	> 20	clean transition
150704.121	3 <sub>0,3</sub> → 3 <sub>1,3</sub>	E	28	19.0	-4.7330	3.1	127	8	clean transition
150704.173	2 <sub>0,2</sub> → 2 <sub>1,2</sub>	E	20	12.3	-4.7266	3.1	328	19	clean transition

**Table 10.** Lines of anti-<sup>13</sup>CH<sub>3</sub>CH<sub>2</sub>OH detected toward G+0.693 with their corresponding spectroscopic information and parameters derived from the LTE fit.

Rest frequency (MHz)	QNs	g <sub>u</sub>	E <sub>u</sub> (K)	log A <sub>ul</sub> (s <sup>-1</sup> )	rms (mK)	∫ T <sub>A</sub> * dν (mK km s <sup>-1</sup> )	SNR	Comments
32509.32	4 <sub>1,3</sub> → 4 <sub>0,4</sub>	9	8.2	-6.4293	1.3	134	19	clean transition
40435.51	6 <sub>1,5</sub> → 6 <sub>0,6</sub>	13	17.0	-6.2050	1.5	67	8	slightly blended with unidentified transition
44748.194	4 <sub>0,4</sub> → 3 <sub>1,3</sub>	9	6.0	-6.3778	2.1	100	9	clean transition
82170.297	6 <sub>0,6</sub> → 5 <sub>1,5</sub>	13	13.1	-5.4772	3.5	121	6	blended with unidentified transition
82223.219	3 <sub>2,2</sub> → 3 <sub>1,3</sub>	7	6.0	-5.5620	2.8	130	9	clean transition
102934.258	5 <sub>1,5</sub> → 4 <sub>0,4</sub>	11	8.2	-5.1178	2.6	253	18	clean transition
113369.368	2 <sub>2,0</sub> → 1 <sub>1,1</sub>	5	2.1	-4.9878	6.8	262	7	clean transition
143297.176	4 <sub>2,3</sub> → 3 <sub>1,2</sub>	9	6.3	-4.8286	2.2	216	18	clean transition
144465.114	8 <sub>1,8</sub> → 7 <sub>0,7</sub>	17	22.7	-4.6339	1.7	81	9	blended with unidentified transition

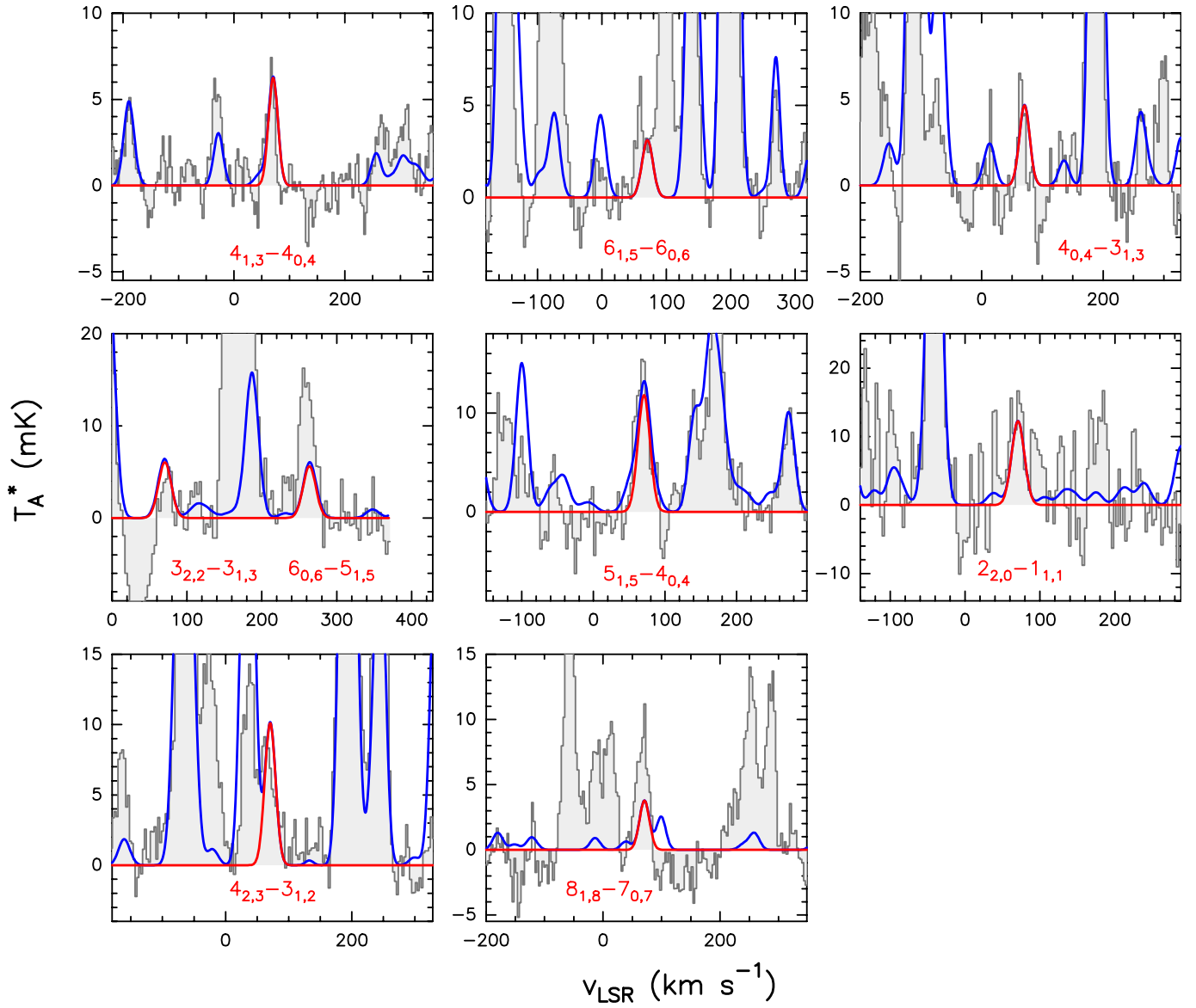


**Figure 6.** Selected lines of **anti- $^{13}\text{CH}_3\text{CH}_2\text{OH}$**  detected toward G+0.693. Black, red and blue lines represent the observational data, the individual lines of  $^{13}\text{CH}_3\text{CH}_2\text{OH}$  and the global fit with all species, respectively.